Electronic Supplementary Material (ESI) for Nanoscale Advances.

Supporting Information

A Combined Experimental and Molecular Simulation Study on Stress Generation Phenomena During Ziegler-Natta Polyethylen Catalyst Fragmentation Process.

Antonio De Nicola,[a] Vasileios Touloupidis,[c] Vasileios Kanellopoulos,[c] Alexandra R. Albunia,[c*] Giuseppe Milano[b*]

[a]Scuola Superiore Meridionale, Largo San Marcellino 10, 80132 Napoli, Italy.

[b]Dipartimento di Ingegneria Chimica, dei Materiali e della Produzione Industriale, Università degli Studi di Napoli Federico II, 80125 Napoli, Italy.

[c]Innovation & Technology, Borealis Polyolefine GmbH, 4021 Linz, Austria

1 Models and Computational Details

1.1 United-Atom Polyethylene Model

Most of the atomistic force-field, included the United Atoms (UA) with non-explicit treatment of hydrogen atoms, are based on the reproduction of structural and thermodynamic properties of the polymer melt. The most adopted force-fields to model alkane chains include the PSY[1] (Paul, Yoon and Smith), his modification made by Waheed *et al.,*[2] the force-field developed by Yamamoto[3,4] and the TraPPE-UA.[5–7] To model the polyethylene (PE) bulk we adopted a united-atoms (UA) representation which combines hydrogens and carbon of each CH_2 or CH_3 moiety into a single site. By using UA model most of the conformational degrees of freedom of a fully explicit atom model are preserved. The TraPPE-UA force field, originally proposed by Siepmann,[8] has been selected as force-field (FF). In particular, TraPPE-UA force-field is optimized to reproduce of the vapor-liquid coexistence curves (VLCC) of *n*-alkanes and a variety of melt phase structures and dynamical properties as well as the structure, melting point and mass density.[8] In Figure S1, a single PE chain (represented by united atoms) site is reported.

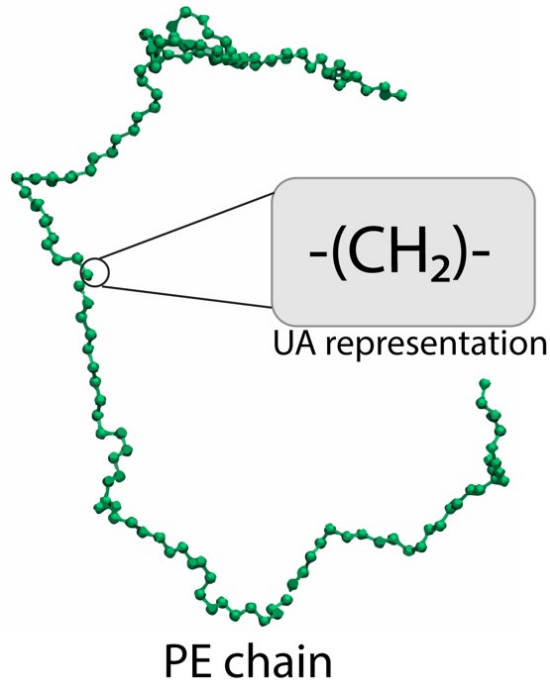

Figure S1. UA representation of a single PE chain. Each UA site represents a CH_2 unit.

The non-bonded interactions between sites of PE model are described by the Lennard-Jones potentials (eq. S1)

$$u(r_{ij}) = 4\epsilon_{ij}\left[\left(\frac{\sigma_{ij}}{r_{ij}}\right)^{12} - \left(\frac{\sigma_{ij}}{r_{ij}}\right)^{6}\right] \qquad \text{(eq. S1)}$$

Where r_{ij}, ϵ_{ij}ij and σ_{ij} are the distance between two sites *i* and *j*, the energy depth and site size, respectively. The bonded interactions, including bonds, angle and dihedral angle, are described the following functional forms:

$$E_{BOND} = K_b(r - r_0)^2 \qquad \text{(eq. S2)}$$

Were r_0 is the equilibrium bond distance fixed at 0.154 *nm*, while the stiffness of the harmonic potential K_b has been set to 188100 *kJ/mol nm*^{2}.

$$E_{ANGLE} = K_a(\theta - \theta_0)^2 \qquad \text{(eq. S3)}$$

Were θ_0 is the equilibrium bond distance fixed at 114˚, while the stiffness of the harmonic potential K_a = 285.6 *kJ/mol rad*^{2}. The torsional potential between four consecutive sites (CHx-CH_2-CH_2-CHx, x=2,3) is given by:

$$E_{TORSION} = \sum_{i=0}^{n=3} C_i cos^i(\emptyset) \qquad \text{(eq. S4)}$$

Where the coefficients C_i have values of: C_0 = 8.39 (kJ/mol), C_1 = 16.77 (kJ/mol), C_2 = 1.13 (kJ/mol), C_3 = -26.29 (kJ/mol).

1.2 System Description and Preparation of initial Melt Structures.

The PE samples are composed of 60 chains, each one containing 150 CH_x UA sites (where $x = 2$ for intrachain and 3 for the terminal groups). The initial configurations were generated at the density of 0.79 g/cm^3 which is equal to the experimental density of PE at 500 K.[9] An orthorhombic cell has been set and the Periodic Boundary Conditions (PBC) were applied in all *x,y,z* directions. All the systems have been pre-equilibrated at 500 K (150 *ns*) in the NVT ensemble by using the hybrid particle-field (hPF) technique and following the procedure reported by De Nicola et al.[10] for the pre-equilibration step, the OCCAM-MD code[11] has been used. Further short equilibration, starting from the final configurations obtained from hPF simulations, was performed along 20 *ns* of standard MD simulations in *NVT* ensemble (500 K). The short equilibration and the production runs were all performed using the GROMACS package.[12] For the production runs, the simulations were performed in the NPT ensemble, with a constant pressure set to 1 atm. The Berendsen barostat algorithm was employed to control the pressure (with a relaxation time τ_P of 1.0 *ps)*. The temperature of was controlled with the velocity rescaling[13] algorithm with a relaxation time (τ_T) of 0.5 *ps*. A time step of $\Delta t = 2$ *fs* has been used for all simulations, while the Lennard-Jones were truncated over a cut-off distance $r_{cut\text{-}off}$ = 1.4 nm.

1.3 Semi-crystalline PE Bulk

The crystallization of a PE bulk can be achieved by cooling, at constant rate, an amorphous system. To control the crystallization of the PE bulk we calculated the crystallization temperature T_c typical of the proposed model. To this aim, eighteen independent simulations of a sample composed of 60 PE chains were performed in a temperature range from 500 to 280 K. In Figure S2, the mass bulk density is reported in the whole investigated range. We found an abrupt increase of density, from

the amorphous phase (~860 kg/m^3) to the semi-crystalline (~ 930 kg/m^3), in a narrow temperature range of two degrees (see the inset of Figure S2 between 305 and 303 K). From the behavior of mass density *vs* the temperature we can conclude that the T_c of our model is in between 303 and 305 K.

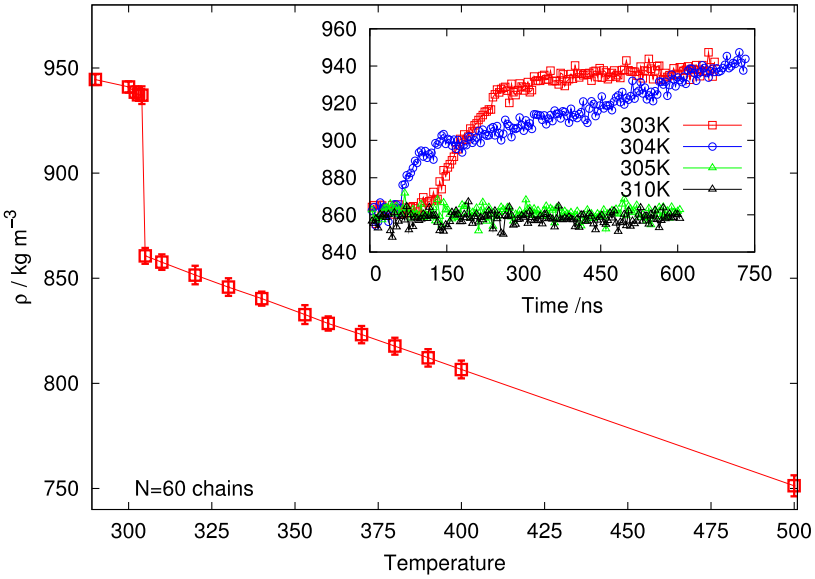

Figure S2. Mass density as function the temperature. Each point represents three independent runs.

How fast the system is cooled down is crucial to control the crystallization process. As an example, if the cooling rate is too high a glass state is produced instead of crystal structure.[14] In order to obtain a reproducible crystal formation and to control the degree of crystallinity too, we need an adequate the cooling rate. In Figure S3, a cooling rate of 22 $K\,ns^{-1}$ is used to obtain a semi-crystalline PE sample. As can be seen, the mass density of the polymer increases up to ~ 940 kg/m^3 typical of a first order transition liquid-solid.

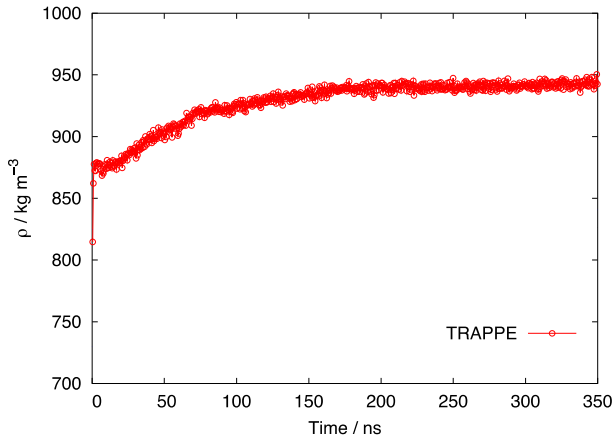

Figure S3. Mass density of PE polymer melt during the quenching procedure. The cooling rate applied to the system reported in figure is 22 K ns^{-1}. The MD run has been performed in NPT ensemble.

In the following, we verified that the degree of crystallinity is controlled by the cooling rate. Especially, we found that a cooling rate range from 22 K ns-1 to 8.8 K ns-1 give us a crystallinity degree going from 67 to 71 %, which is in the range of interest our investigation. The calculation of crystallinity is discussed in the following. In Figure S4, the crystal formation obtained via ultrafast quenching of PE melt from 500 K to 280 K is reported. The crystallization process was monitored via time evolution of mass density (Figure S3) and potential energy for chain, reported in and S4A. The abrupt increase of the mass density, in the short time range 40-120 ns, clearly indicates a transition from an amorphous to a semi-crystalline phase. Looking at the potential energy for chain, we observe three distinct time periods (Figure S4a). A fast re-equilibration of potential energy from the initial configuration (~5 ns) followed by an induction period between 5-100 ns. During this time, fluctuations of potential energy and density favors the nucleation and the growth of crystal domains, as shown in the snapshot sequence reported in Figure S4, from 20 to 100 ns. Finally, stable crystal domains are found after 150 ns. As the crystal domains grow in time, the orientational order parameter P2 increments too from 0.3 up to 0.7 (Figure S4b). is defined as $P_2 = \langle 3cos\theta_{ik}^2 - 1/2 \rangle$where θ_{ik} is the angle between the vector formed by (i-1)th to (i+1)th bead, and the vector formed by (k-1)th to (k+1)th bead. The average is taken over all pairs of chords and over all PE chains. As can be seen from representative snapshots at increasing simulation time (see left panel of Figure S4), the crystal domains are quickly formed in about 100 ns. The configuration at 280 ns shows two different crystalline regions connected by a disordered amorphous layer.[15] A

close examination of the resulting equilibrium configurations shows also the typical hexagonal packing of PE chains,[2,16–18] as reported in the left panel of Figure S4.

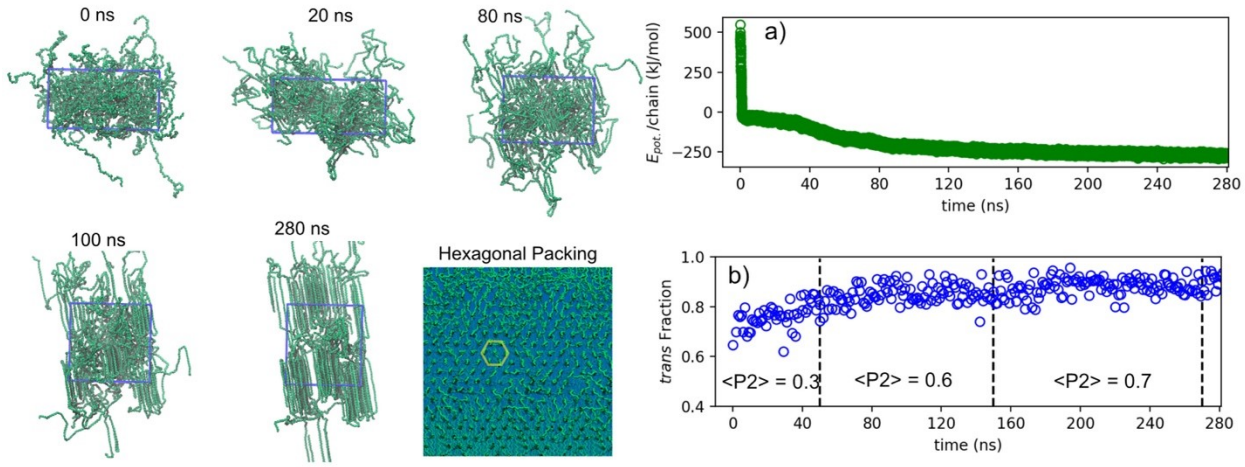

Figure S4. Left of the figure, a sequence of snapshots took during the fast quenching of the PE melt are reported. The blue box represents the orthorhombic simulation box. In the last snapshots, next to those at 280 ns, a view of the PE chains along the crystal orientation is reported to highlight the typical hexagonal pathway of a PE polymer crystal. In the panels *a)* and *b)* and *c)*, the time evolution of potential energy for chain and trans fraction of PE chains are reported.

The degree of crystallinity is defined as:

$$\alpha_{\%} = \frac{\rho_K(\rho_S - \rho_A)}{\rho_S(\rho_K - \rho_A)} \times 100 \qquad \text{(eq. S5)}$$

Where ρ_K is the density of the perfect crystal, ρ_s is the density of the semi-crystalline system, and ρ_A is the mass density of the PE amorphous phase.

To calculate the degree of crystallinity of a semi-crystalline system, the density a perfect PE crystal of is needed. To this aim, we built a large slab of perfect PE crystal by replica (in *x, y, z* direction) of the experimental unit cell.[19] To get a suitable initial configuration for the MD simulation, The unit cell of PE has been replicated ten times in each *x, y, z* direction. The final systems, from the replica, consist of 50 PE chains in a box size of 3.92324 x 2.9339 x 5.06577 *nm.* In Figure S5A, the top and lateral views of the replica PE crystal are shown.

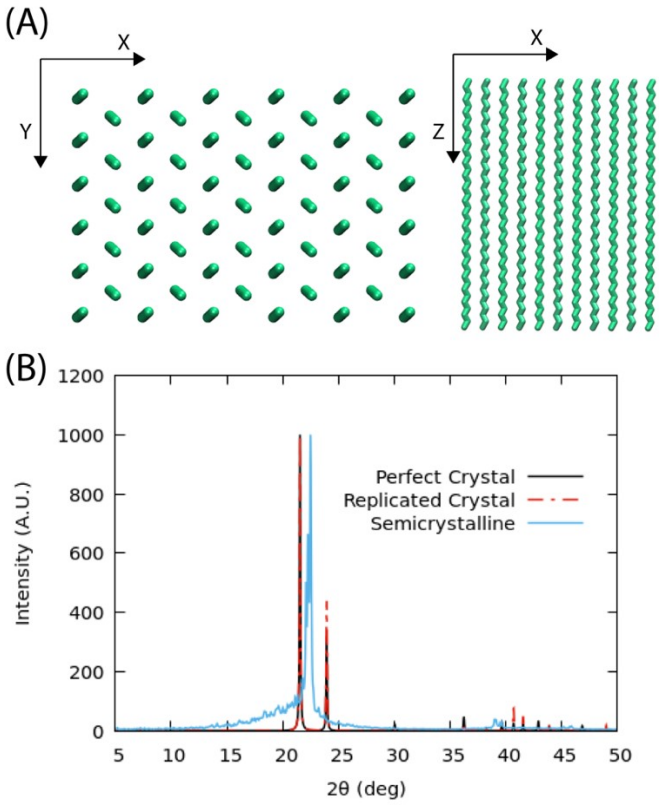

Figure S5. (A) Top (*xy* plane) and Lateral (*xz* plane) views of the replicated PE crystal. (B) X-Ray pattern comparison between the perfect crystal structure (black line), replicated crystal (red point line) and semi-crystalline (blue line).

As can be seen from Figure S4B, the X-Ray pattern calculated on the perfect PE crystal (from experimental coordinates, and the replicated PE crystal systems, are identical. The X-Ray pattern calculated for the semi-crystalline system (at 67 % of degree of crystallinity via eq. S5) agrees with experimental pattern measured on a similar system.[19]

1.4 Pressure Response due to PE mass increase

We investigate how different phase states of PE behave, in terms of pressure increment ($\Delta P = P_{n+1} - P_0$) where n is the initial number of monomer and P_0 corresponds to the initial equilibrium pressure of 1 atm in absence of monomer insertion. We considered three systems of pure polymer bulk of PE in the amorphous, semi-crystalline and crystalline phase. All simulations have been performed at constant number of particles in the NVT ensemble and in Periodic Boundary Conditions (PBC). It means that the polymer has not interface. Since the number of particles is kept constant, the "virtual" increase of the polymer is obtained by gradually shrinking

the box volume and increasing, hence, the mass density. Then, the ΔP increment is registered at each decrement step of the volume, Figure S6. The crystal-domains growth along preferential directions for semi- and perfect crystal PE polymer phase makes their conformations anisotropic (see the preferential grow direction with respect to the axes in the snapshots of Figure S6). For that reason, the volume shrinking is applied in the x, y and z directions one by one. It means that for a set of simulations the volume is reduced by shortening only one direction, leaving the others two fixed to the original equilibrium value. As can be seen in the plot of Figure S6, for amorphous PE the ΔP increment is modest compared to those observed for semi- and crystalline phases. It means that for a set of simulations the volume is reduced by shortening only one direction, leaving the others two fixed to the original equilibrium value. As can be seen in the plot of Figure S6, for amorphous PE the ΔP increment is modest compared to those observed for semi- and crystalline phases. Comparable values of ΔP_α components (α=X, Y, Z) show an isotropic accumulation of the stress (equal in all directions). Differently, for the crystal phase the Z direction (aligned in the same direction of crystal domain) show a huge increase of ΔP. In fact, a very small increment of the density corresponding to an addition of 0.5 monomers causes a pressure increase up to 100 bar, see the green open square in the plot of Figure S6. For the other two directions (Y and X) the ΔP increases similarly, just happens at a higher number of added monomers. The semi-crystalline phase shows similar trends as for the crystal phase. The ΔP increase is registered after the addition of about two monomers. Also, in this case the Z direction shows the largest increase, see the yellow open square in Figure S6. The main difference between semi- and crystalline phase is due to the presence, in the first, of a layer of amorphous PE. Especially, the larger number of accessible chain conformations, due to the higher chain flexibility of amorphous phase, reduces the stress increment caused by an increase of the density. For the same reason, to observe a stress accumulation in the amorphous phase, an addition of more monomers is needed compared to semi- and crystalline phase.

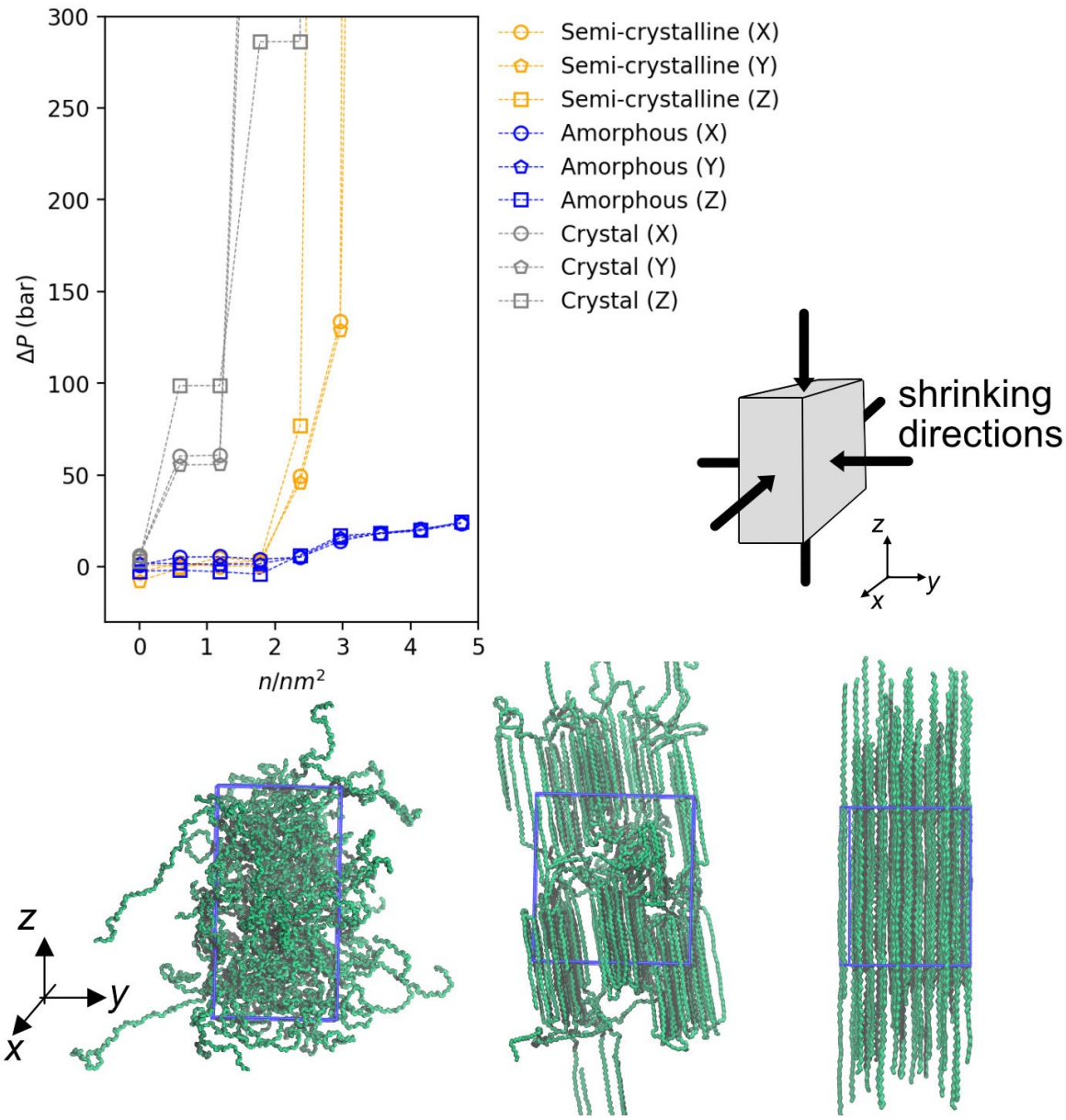

Figure S6. ΔP values as function of the inserted number of monomers calculate for amorphous, semi-crystalline and crystalline phase of PE. On bottom, three representative snapshots of different PE physical states are reported to show the crystal domain orientation. A scheme showing the box shrinking directions is also included in the figure. For all simulated systems, a 0.05% decrement of the box is applied at each step.

1.5 $MgCl_2$ Catalyst Support Model

$MgCl_2$ is currently used as a support for the active titanium center in the olefin polymerization via Ziegler-Natta. In particular, $MgCl_2$ is a layered system with trigonal $P\bar{3}m1$ space group (primitive hexagonal cell[20–22]) described by three structural parameters a = 3.641 Å, c = 5.927 Å, u = 0.23 Å.

The Mg and Cl atoms are arranged in hexagonal layers which pack in sequence -*Cl-Mg-Cl-Cl-Mg-Cl-* along *u* direction, as reported in Figure S7A.

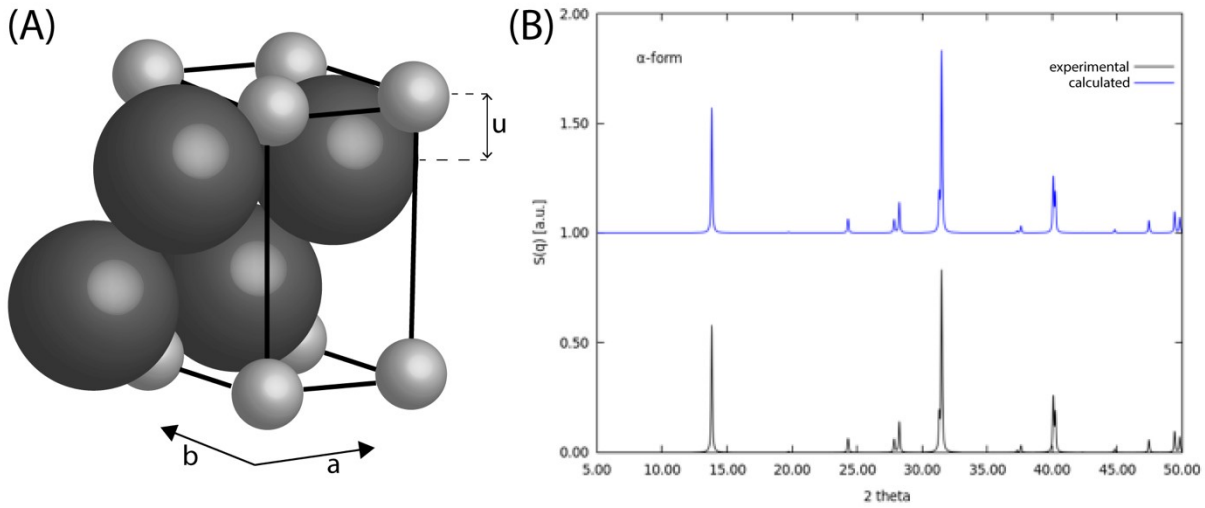

Figure S7. A unit cell of $MgCl_2$. The atoms are draw as sphere, Cl in dark grey and Mg in light grey. (B) Comparison between X-Ray pattern of the $MgCl_2$ crystal measured (black line) and calculated (blue line) from MD model.

In order to have a size of the crystal that is suitable for the MD simulations, we replicated the unit cell of the $MgCl_2$ crystal 10 times in each *x, y, z* direction. We obtained an initial structure composed of 6000 atoms with a box volume of 143.1 $Å^3$, corresponding to a density = 2.134 g/cm^3 (equal to the experimental value[23] of 2.134 g/cm^3). The consistency of the replicated crystal structure has been checked by comparing the X-Ray pattern with the respect to experimental one. As can be seen in Figure S7B, the X-Ray pattern of the replicated crystal (blue line) perfectly matches the experimental one (black line). Views of planes of the replicated crystal slab are reported in Figure S8.

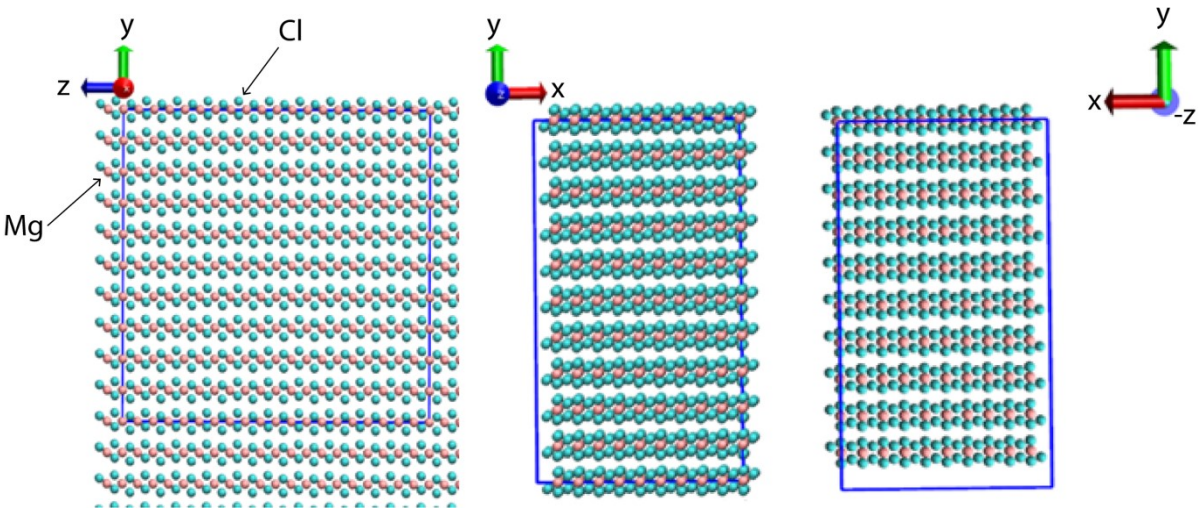

Figure S8. Different view of replicated $MgCl_2$ crystal.

To the best of our knowledge, for this compound, few studies about classical MD force-field have been reported in literature. We did not find suitable force-field for the anhydrous $MgCl_2$ crystal. In addition, only some studies are reported about $MgCl_2$ *$[H_2O]n$ crystal at different hydration level.[24]

In our first attempt we performed MD simulation of the $MgCl_2$ crystal by using OPLS-AA force field,[25,26] which is compatible with the TraPPE-UA force field we adopted for the PE polymer melt. We performed an additional simulation using the IOD force field,[24] that has been demonstrated to reproduce the hydrated crystal structure of $MgCl_2$ *$[H_2O]n$. All simulations have been performed using GROMACS package[12] in *NPT* ensemble with a time step of $\Delta t = 2$ *fs*. The velocity-rescale[13] thermostat with a relaxation time (τ_T) of 0.5 *ps*. The Lennard-Jones potential was truncated at the cut-off distance $r_{cut\text{-}off} = 1.4$ nm, and the long range electrostatic interaction are computed by using Particle Mesh Ewald method.[27]

Both force fields the OPLS[26] and IOD, failed to reproduce the bulk density of the anhydrous $MgCl_2$ crystal. The calculated mass density is underestimated of about 42% with respect to experimental value[23] of 2.134 g/cm^3, as reported in Figure S9A.

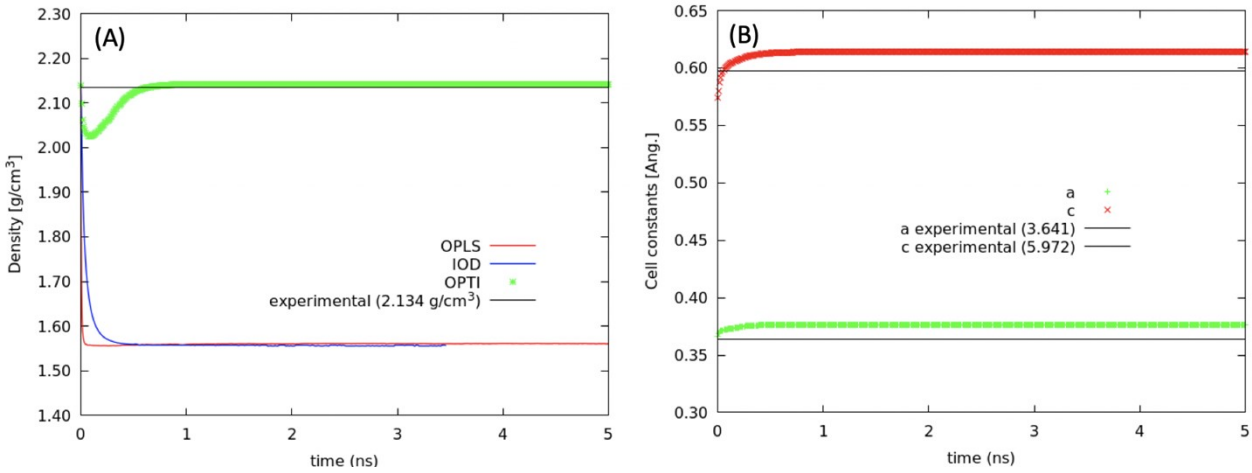

Figure S9. Time evolution of: (A) Mass density for the MD simulations of $MgCl_2$ anhydrous crystal, (B) Crystal lattice constants *a, b, c* from the OPTI force field simulation.

It is worth noting that for both OPLS and IOD force fields the radius ratio **R** (defined as the ratio between the cation and anion particles) is at the extreme of the experimental range 0.4< **R** <0.73 (see Table S1). Based on geometrical considerations, we tuned the initial OPLS force-field parameters to have a **R** closer to 0.5.

Table S1. Parameters for OPLS, IOD and optimized (OPTI) force field used for the $MgCl_2$ crystal.

Force-Field	Atom	σ *(nm)*	ε *(kJ/mol)*	**R** (r_a/r_c)	Charge
OPLS	Mg	1.64447×10^{-1}	0.36611×10^{-1}	0.37	+2
	Cl	4.41724×10^{-1}	4.92833×10^{-1}		-1
IOD	Mg	2.48600×10^{-1}	6.2400×10^{-2}	0.64	+2
	Cl	3.85200×10^{-1}	0.22240×10^{-1}		-1
OPTI	Mg	1.80000×10^{-1}	1.60000×10^{-1}	0.48	+2
	Cl	3.70000×10^{-1}	0.16000×10^{-1}		-1

From the MD simulations performed with the tuned OPTI force field, we calculated and compared the mass bulk density and the crystal cell parameters for the $MgCl_2$ system (Figure S9A-B). As can be seen from the figure, we are able to reproduce the mass density of the crystal within an error of 0.6 % and we have a small deviation of the *a* (+1.1 %) and *c* (+1.3 %) cell parameters compared with experimental values.

Snapshots of crystal bulk of MgCl2, simulated at 353 K (to check the stability of the crystal at the conditions we are interested) are reported in Figure S10.

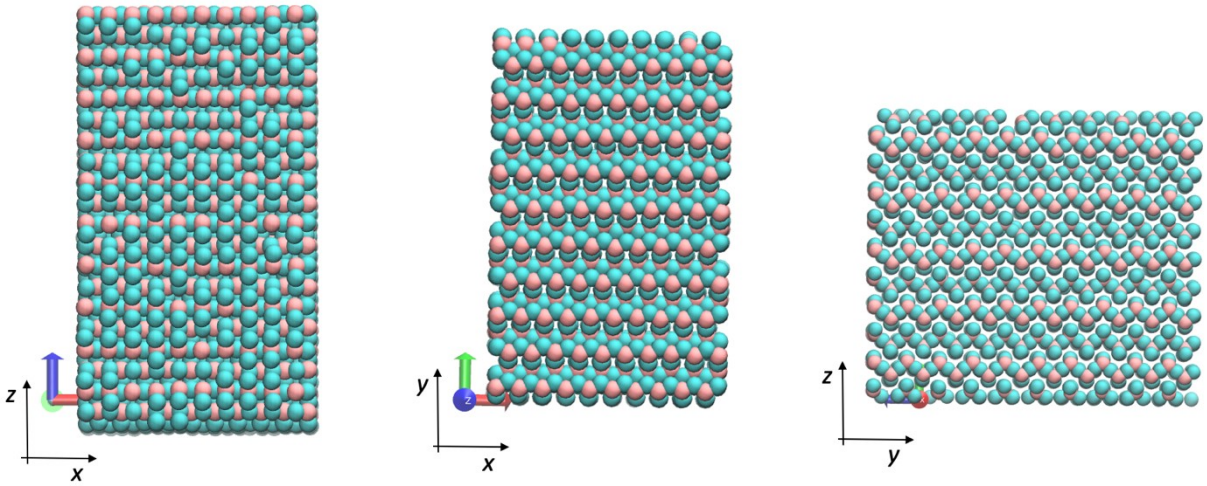

Figure S10. Snapshots from MD simulation, using the OPTI force field, simulated at 353 K.

1.6 $MgCl_2$ support, face [110].

Is general accepted that the most convenient catalytic surface of $MgCl_2$ is the that one obtained from the cut [110].[28,29] At the best of our knowledge, there are no works in literature investigating the stability of the $MgCl_2$ [110] surface plane by using atomistic force field. In order to check the stability of $MgCl_2$ crystal exposing the plane [110], which is a function of the model parameters and the system size, we extract from a crystalline bulk of $MgCl_2$ a slab with a thickness of 4 nm and the plane [110] of 13.0 x 13.3 nm. Then, a MD simulation at 353 K was performed to check the thermal stability of the crystalline slab in contact with PE chains. To this aim, 111 polymer chains were randomly placed on top of the crystalline plane (cut [110]). The bulk density of the PE has been initially set at 820 kg/m^3, according to the density of the PE melt. The results of the MD simulations are reported in Figure S11. As first we verified that the crystalline structure is stable at 353 K, which the highest temperature we investigated. Only a slightly displacement from the initial reticular site is found for both magnesium and chlorine atoms. More quantitatively, the stability of the $MgCl_2$ slab is evaluated by comparing the mass density profile calculated for crystal/void interface and crystal/PE interface (Figure S11B). As can be seen from the figure, the density profiles of the crystal slab are in practice equal (black line $MgCl_2$/PE interface, green

segmented line $MgCl_2$/void interface). The PE chains result to be strongly attracted by the chlorine atoms belonging the surface (red segmented line).

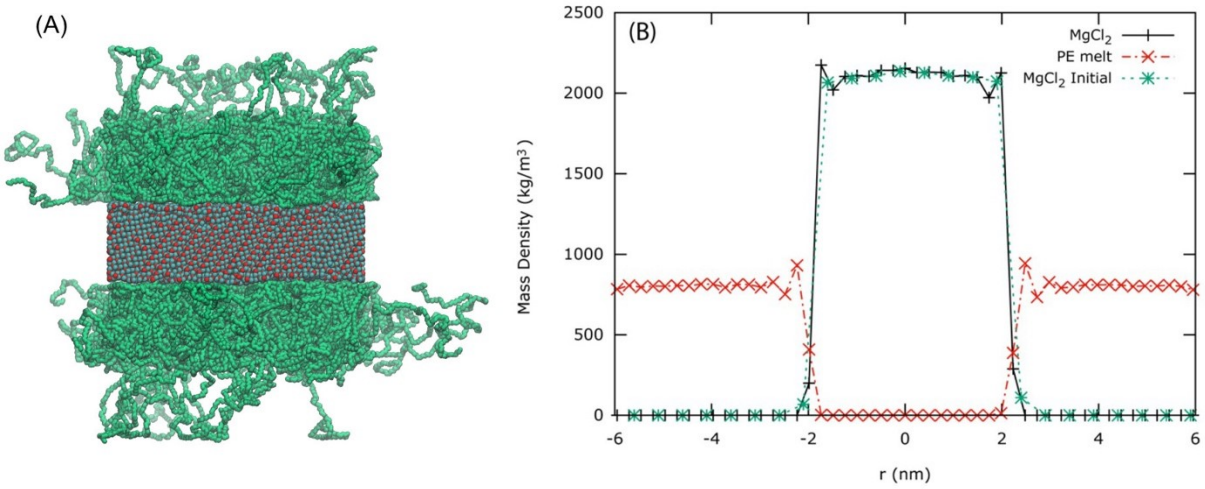

Figure S11. (A) snapshot of $MgCl_2$ [110] with PE chains (in grey) of a simulation of 5 ns long. (B) Mass density profile calculated with the respect to the normal direction of $MgCl_2$ surface for the $MgCl_2$/void interface (green line), $MgCl_2$/PE interface (black line) and PE chains (red line).

1.7 Systems Composition

Table S2. Simulated Systems Composition

System	PE chains	mon./chain	Mg^{2+}	Cl^-	Box [x,y,z] (nm)	Temp. (K)	Time (ns)
1	60	150	-	-	15.00000; 10.43319; 12.00000	353	5000
2	60	150	-	-	15.00000; 7.245210; 12.00000	313	5000
3	50	40	-	-	3.943240; 2.309390; 4.60563	305	500
4	-	-	20000	40000	13.00000;	313	250

					13.30000; 20.00000	353	250
5	-	-	9360	18720	13.27001;	313	250
					13.13060; 4.000000	353	250
6	111	150	9360	18720	13.27001;	313	300
					13.13060; 12.40090	353	300

2 Additional Results

In absence of heterogeneities, i.e. the crystallization from an homogeneous polymer bulk, the nucleation take place randomly. In the following, a set of isosurfaces calculated from a PE bulk are reported, in Figure S12. The isosurface represent a volume data V which is equal to a certain specified value (in our case this value is the mass density of the PE 1.3 larger than the final equilibrated semicrystalline phase). Isosurfaces are computed by dividing the system in cells, with a fixed lengths *lx, ly, lz* and volume (V_{cell}). According to the particle assigned to each cell, the corresponding cell density is computed. A density cut-off is used to represent the isosurfaces reported in the following figures.

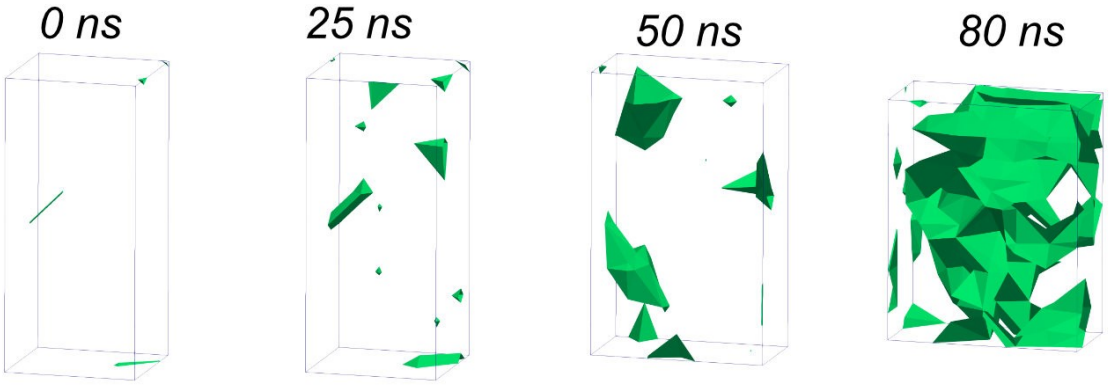

Figure S12. Density isosurfaces of PE (in green) at different stages of crystallization.

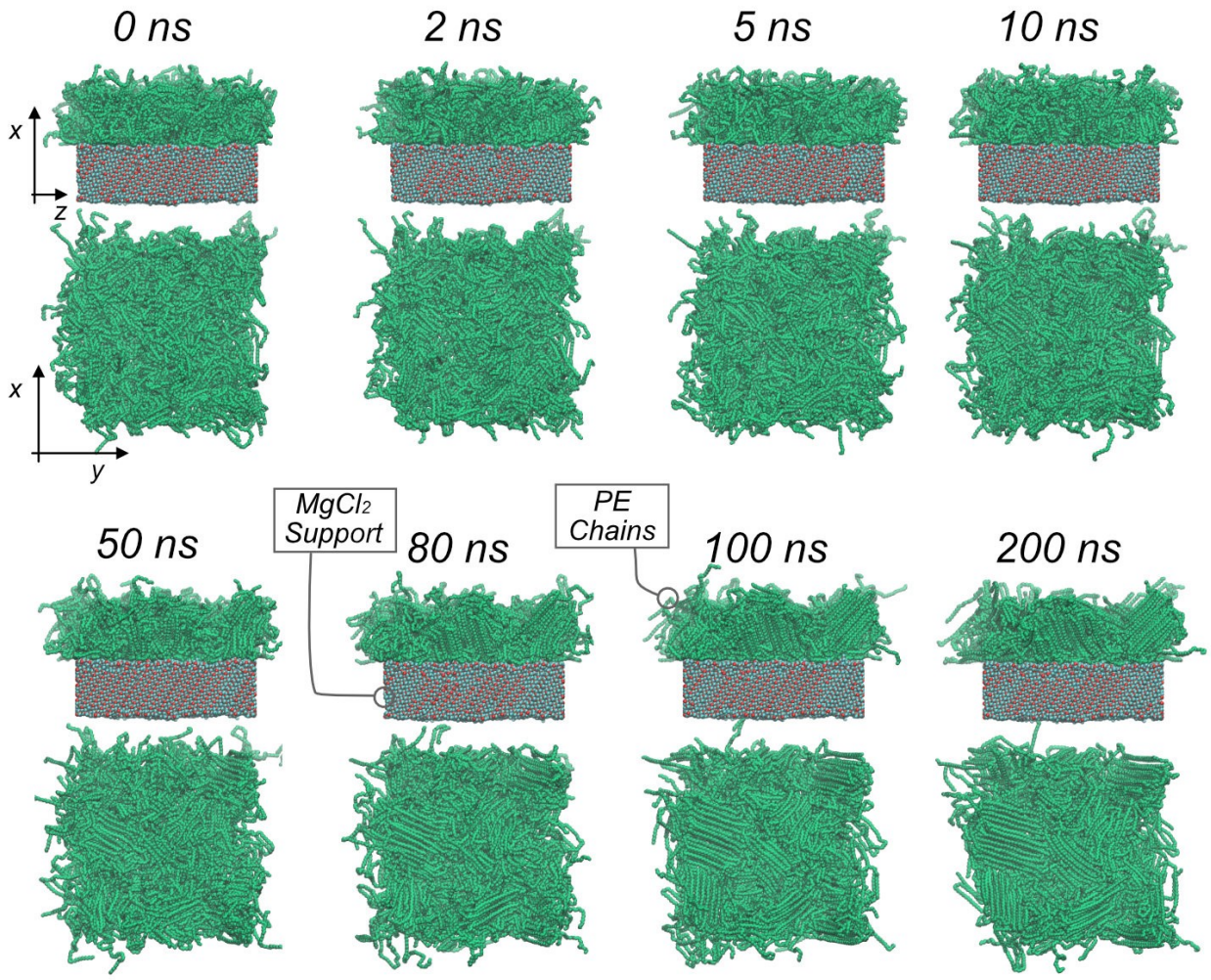

Figure S13. Snapshot sequence showing the formation of PE crystal domain during the quenching process.

In Table S3, a comparison between the melting temperature (Tm1), heat of fusion (DH1) and bulk density ρ, is reported for sample obtained at constant temperature of 50°C and at different condition of activity (A) and concentration and type of additives.

Table S3. A=activity of catalyst, F = flowability, ρ= bulk density. All samples have been produced at 50°C.

Sample	Additive	A $\frac{kg_{PE}}{g_{CAT}\,h}$	Tm1 °C	DH1 J/g	ρ g/mL	F	Mw* kg/mol
1	9 mol% (C2)	5.53	143.23	206.0	0.279	none	1509
2	14 mol% (C2)	12.2	143.29	195.8	0.320	none	1917
3	14 mol% C2, 11.2 mol/kmolH_2	10.0	140.14	200.4	0.345	yes	1275
4	14% mol C2, 70 mol/kmol (C6),	12.3	141.02	183.5	0.430	yes	1350

*For such high Mw values, the error associated with the GPC measurement can be relatively high, due to the difficulty to dissolve the longer chains. The numbers should be considered rather as indicative of the trend.

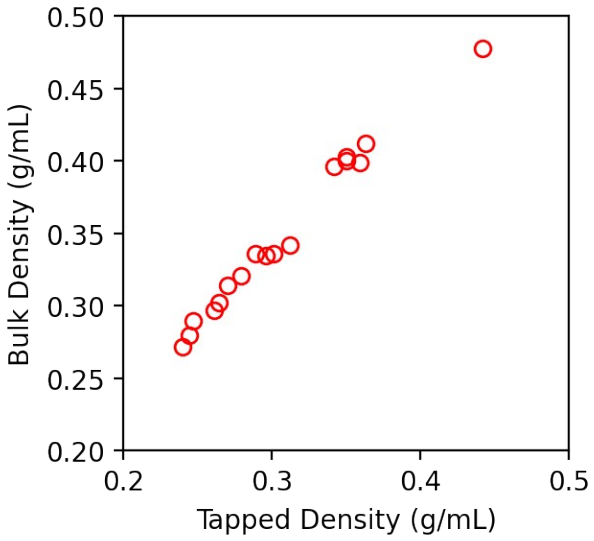

Figure S14. Correlation between Tapped and Bulk densities.

3 Bench-scale polymerization

Bench-scale polymerizations typically take place in a 5 L jacketed reactor, equipped with a helical stirrer. The reactor is operated in a semi-batch mode: all reaction species can be initially batch-fed, there is no outflow, nevertheless, monomers and hydrogen can be further introduced in the reactor continuously. This way, pressure is maintained in the desired set-point level, always compensating the pressure decrease due to monomer consumption. The polymerisation runs are conducted in slurry mode, using propane as diluent, and using a $MgCl_2$ based ZN catalyst with an average size of 15μm. More details can be found in the work of Touloupidis et al., 2020.[30]

4 References

(1) Paul, W.; Yoon, D. Y.; Smith, G. D. An Optimized United Atom Model for Simulations of Polymethylene Melts. *The Journal of Chemical Physics* **1995**, *103* (4), 1702–1709. https://doi.org/10.1063/1.469740.

(2) Waheed, N.; Lavine, M. S.; Rutledge, G. C. Molecular Simulation of Crystal Growth in *n* -Eicosane. *The Journal of Chemical Physics* **2002**, *116* (5), 2301–2309. https://doi.org/10.1063/1.1430744.

(3) Yamamoto, T. Molecular Dynamics of Reversible and Irreversible Melting in Chain-Folded Crystals of Short Polyethylene-like Polymer. *Macromolecules* **2010**, *43* (22), 9384–9393. https://doi.org/10.1021/ma101777d.

(4) Yamamoto, T. Molecular Dynamics of Polymer Crystallization Revisited: Crystallization from the Melt and the Glass in Longer Polyethylene. *The Journal of Chemical Physics* **2013**, *139* (5), 054903. https://doi.org/10.1063/1.4816707.

(5) Martin, M. G.; Siepmann, J. I. Transferable Potentials for Phase Equilibria. 1. United-Atom Description of *n* -Alkanes. *J. Phys. Chem. B* **1998**, *102* (14), 2569–2577. https://doi.org/10.1021/jp972543+.

(6) Martin, M. G.; Siepmann, J. I. Novel Configurational-Bias Monte Carlo Method for Branched Molecules. Transferable Potentials for Phase Equilibria. 2. United-Atom Description of Branched Alkanes. *J. Phys. Chem. B* **1999**, *103* (21), 4508–4517. https://doi.org/10.1021/jp984742e.

(7) Chen, B.; Siepmann, J. I. Transferable Potentials for Phase Equilibria. 3. Explicit-Hydrogen Description of Normal Alkanes. *J. Phys. Chem. B* **1999**, *103* (25), 5370–5379. https://doi.org/10.1021/jp990822m.

(8) Chen, B.; Siepmann, J. I. Transferable Potentials for Phase Equilibria. 3. Explicit-Hydrogen Description of Normal Alkanes. *The Journal of Physical Chemistry B* **1999**, *103* (25), 5370–5379. https://doi.org/10.1111/j.1365-2958.2004.04444.x.

(9) Dee, G. T.; Ougizawa, T.; Walsh, D. J. The Pressure-Volume-Temperature Properties of Polyethylene, Poly(Dimethyl Siloxane), Poly(Ethylene Glycol) and Poly(Propylene Glycol) as a Function of Molecular Weight. *Polymer* **1992**, *33* (16), 3462–3469. https://doi.org/10.1016/0032-3861(92)91104-A.

(10) De Nicola, A.; Kawakatsu, T.; Müller-Plathe, F.; Milano, G. Fast Relaxation of Coarse-Grained Models of Polymer Interphases by Hybrid Particle-Field Molecular Dynamics: Polystyrene-Silica Nanocomposites as an Example. *European Physical Journal: Special Topics* **2016**, *225* (8–9), 1817–1841. https://doi.org/10.1140/epjst/e2016-60127-0.

(11) Zhao, Y.; De Nicola, A.; Kawakatsu, T.; Milano, G. Hybrid Particle-Field Molecular Dynamics Simulations: Parallelization and Benchmarks. *Journal of Computational Chemistry* **2012**, *33* (8), 868–880. https://doi.org/10.1002/jcc.22883.

(12) Berendsen, H. J. C.; van der Spoel, D.; van Drunen, R. GROMACS: A Message-Passing Parallel Molecular Dynamics Implementation. *Computer Physics Communications* **1995**, *91* (1), 43–56. https://doi.org/10.1016/0010-4655(95)00042-E.

(13) Hoover, W. G. Canonical Dynamics: Equilibrium Phase-Space Distributions. *Phys. Rev. A* **1985**, *31* (3), 1695–1697. https://doi.org/10.1103/PhysRevA.31.1695.

(14) Barrat, J.-L.; Baschnagel, J.; Lyulin, A. Molecular Dynamics Simulations of Glassy Polymers. *Soft Matter* **2010**, *6* (15), 3430–3446. https://doi.org/10.1039/B927044B.

(15) Chen, H. Y.; Chum, S. P.; Hiltner, A.; Baer, E. Comparison of Semicrystalline Ethylene-Styrene and Ethylene-Octene Copolymers Based on Comonomer Content. *J. Polym. Sci. B Polym. Phys.* **2001**, *39* (14), 1578–1593. https://doi.org/10.1002/polb.1130.
(16) Haselwander, Th. F. A.; Heitz, W.; Krügel, St. A.; Wendorff, J. H. Rigid Random Coils: Rotationally Confined Chain Molecules. *Macromolecules* **1997**, *30* (18), 5345–5351. https://doi.org/10.1021/ma970306z.
(17) Fujiwara, S.; Sato, T. Molecular Dynamics Simulations of Structural Formation of a Single Polymer Chain: Bond-Orientational Order and Conformational Defects. *The Journal of Chemical Physics* **1997**, *107* (2), 613–622. https://doi.org/10.1063/1.474421.
(18) Koyama, A.; Yamamoto, T.; Fukao, K.; Miyamoto, Y. Molecular Dynamics Studies on Polymer Crystallization from a Stretched Amorphous State. *Journal of Macromolecular Science, Part B* **2003**, *42* (3–4), 821–831. https://doi.org/10.1081/MB-120021608.
(19) CAMINITI, R.; PANDOLFI, L.; BALLIRANO, P. Structure of Polyethylene from X-Ray Powder Diffraction: Influence of the Amorphous Fraction on Data Analysis. *Journal of Macromolecular Science, Part B* **2000**, *39* (4), 481–492. https://doi.org/10.1081/MB-100100400.
(20) Harrison, N. M.; Saunders, V. R. The Structural Properties of Beta -MgCl 2 ; an Ab Initio Study. *Journal of Physics: Condensed Matter* **1992**, *4* (15), 3873.
(21) Harrison, N. M.; Serc, M. L. The Derivation of Shell Model Potentials for Mgcl2 from Ab Initio Theory. *Molecular Simulation* **1992**, *9* (2), 171–174. https://doi.org/10.1080/08927029208050609.
(22) Lin, J. S.; Catlow, C. R. A. Computer-Modelling Studies on MgCl 2 -Supported Ziegler–Natta Catalysts. *J. Mater. Chem.* **1993**, *3* (12), 1217–1225. https://doi.org/10.1039/JM9930301217.
(23) *CRC Handbook of Chemistry and Physics*, 85th ed.; Taylor and Francis: Boca Raton, F, 2005.
(24) Huinink, H. P.; Zahn, D. Elucidating Water Dynamics in MgCl2hydrates from Molecular Dynamics Simulation. *Solid State Sciences* **2017**, *69*, 64–70. https://doi.org/10.1016/j.solidstatesciences.2017.05.011.
(25) Jorgensen, W. L.; Maxwell, D. S.; Tirado-Rives, J. Development and Testing of the OPLS All-Atom Force Field on Conformational Energetics and Properties of Organic Liquids. *Journal of the American Chemical Society* **1996**, *118* (45), 11225–11236. https://doi.org/10.1021/ja9621760.
(26) Jorgensen, W. L.; Tirado-Rives, J. The OPLS [Optimized Potentials for Liquid Simulations] Potential Functions for Proteins, Energy Minimizations for Crystals of Cyclic Peptides and Crambin. *J. Am. Chem. Soc.* **1988**, *110* (6), 1657–1666. https://doi.org/10.1021/ja00214a001.
(27) Kolafa, J.; Perram, J. W. Cutoff Errors in the Ewald Summation Formulae for Point Charge Systems. *Molecular Simulation* **1992**, *9* (5), 351–368. https://doi.org/10.1080/08927029208049126.
(28) Capone, F.; Rongo, L.; D'Amore, M.; Budzelaar, P. H. M.; Busico, V. A Periodic Hybrid DFT Approach (Including Dispersion) to MgCl2-Supported Ziegler-Natta Catalysts 2: Model Electron Donor Adsorption on MgCl2 Crystal Surfaces. *J. Phys. Chem. C* **2013**, *117*, 24345.
(29) Credendino, R.; Pater, J. T. M.; Correa, A.; Morini, G.; Cavallo, L. Thermodynamics of Formation of Uncovered and Dimethyl Ether Covered MgCl2 Crystallites. Consequences

in the Structure of Ziegler-Natta Heterogeneous Catalysts. *J. Phys. Chem. C* **2011**, *115*, 13322.
(30) Touloupidis, V. Catalytic Olefin Polymerization Process Modeling: Multi-Scale Approach and Modeling Guidelines for Micro-Scale/Kinetic Modeling: Catalytic Olefin Polymerization Process Modeling. Macromol. React. Eng. 2014, 8 (7), 508–527. https://doi.org/10.1002/mren.201300188.